JCTC Journal of Chemical Theory and Computation

Article

pubs.acs.org/JCTC

Exploring the Multidimensional Free Energy Surface of Phosphoester Hydrolysis with Constrained QM/MM Dynamics

Wenjin Li,[†,‡] Till Rudack,[§] Klaus Gerwert,[†,§] Frauke Gräter,*[,†,‡] and Jürgen Schlitter*[,§]

[†]CAS-MPG Partner Institute and Key Laboratory for Computational Biology, Shanghai Institutes for Biological Sciences, Chinese Academy of Sciences, 320 Yue Yang Road, Shanghai 200031, China

[‡]Heidelberg Institute for Theoretical Studies, Schloss-Wolfsbrunnenweg 35, 69118 Heidelberg, Germany

[§]Ruhr-Universität Bochum, Lehrstuhl für Biophysik ND 04, 44780 Bochum, Germany

Supporting Information

ABSTRACT: The mechanism of the hydrolysis of phosphate monoesters, a ubiquitous biological reaction, has remained under debate. We here investigated the hydrolysis of a nonenzymatic model system, the monomethyl phosphate dianion, by hybrid quantum mechanical and molecular mechanical simulations. The solvation effects were taken into account with explicit water. Detailed free energy landscapes in two-dimensional and three-dimensional space were resolved using the multidimensional potential of mean constraint force, a newly developed method that was demonstrated to be powerful for free energy calculations along multiple coordinates. As in previous theoretical studies, the associative and dissociative pathways were indistinguishable. Furthermore, the associative pathway was investigated in great detail. We propose a rotation of an O−H bond in the transition between two pentacoordinated structures, during which an overall transition state was identified with an activation energy of 50 kcal/mol. This is consistent with experimental data. The results support a concerted proton transfer from the nucleophilic water to the phosphate group, and then to the leaving group.

INTRODUCTION

Phosphate monoester hydrolysis is of great biological importance. Among other things, it is involved in the regulation of protein function, energy production, and other biochemical pathways in cells.[1−3] Monomethyl phosphate dianion (MPD) is a phosphate monoester of small molecular weight, the hydrolysis of which is a nonenzymatic reaction which shares great similarity with biologically more important and more complex enzymatic reactions, such as the hydrolysis of GTP in Ras. Thus, it has been intensively investigated.[4−15] As shown in Figure 1, the hydrolysis of MPD involves the ($P-O_W$) bond formation between the oxygen atom of the nucleophilic water (O_W) and the phosphorus atom of MPD (P), and the cleavage of the bond ($P-O_M$) between atom P and one of the oxygen atoms in the methyl group (O_M). Such a reaction, it was proposed, proceeds either by an associative pathway, in which the formation of the $P-O_W$ bond occurs prior to the cleavage of the $P-O_M$ bond via a pentacoordinated transition state (TS; the upper pathway in Figure 1) or by a dissociative pathway in which the cleavage of the $P-O_M$ bond precedes the formation of the $P-O_W$ bond via a TS of metaphosphate (the lower pathway in Figure 1).

Which pathway dominates the hydrolysis reaction has remained elusive, even for the supposedly simple case of MPD. It was suggested that the structural nature of the TSs of these two mechanisms could be distinguished on the basis of the Brønsted linear free-energy relationship, the linear relationship between the logarithm of the observed rate constant and the pK_a of the nucleophile or the leaving group,[18,19] kinetic isotope effects,[1] and the entropy of activation.[20] However, the evidence from these methods, which supported a dissociative mechanism[1,20−22] for the hydrolysis of MPD, was inconclusive after a detailed analysis.[10,12,23] Given the failure of the experimental efforts to provide a clear picture of the

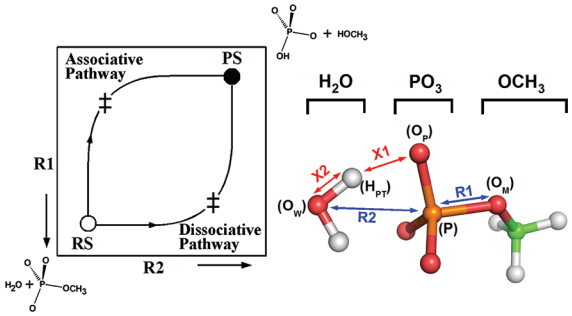

Figure 1. A schematic description of the two limiting pathways for the hydrolysis of monomethyl phosphate dianion. Left: The associative and dissociative pathways are illustrated in a More O'Ferral-Jencks plot,[16,17] and simple representations of the reactant state (RS, ○), transition states (‡), and the product state (PS, ●) are given. Right: MPD and water, the reactant state, are schematically shown. Atoms O_W, O_M, H_{PT}, O_P, and P are labeled, and four reaction coordinates R1, R2, X1, and X2 are defined. O_W: the oxygen atom of water. O_M: one of the oxygen atoms of the methyl group. H_{PT}: the proton in water that transfers to one of the oxygen atoms in the phosphate group. O_P: the oxygen atom in the phosphate group that receives the proton H_{PT}. P: the phosphorus atom of the phosphate group. R1: the distance between O_W and P. R2: the distance between P and O_M. X1: the distance between H_{PT} and O_W. X2: the distance between H_{PT} and O_P.

Special Issue: Wilfred F. van Gunsteren Festschrift

Received: January 12, 2012
Published: April 26, 2012

mechanism, theoretical approaches were employed to estimate the free energy difference of the TSs along both pathways, which seemed to be the only conclusive evidence. In the early stage of the investigation, computational studies in the gas phase supported an associative pathway, while the energy barrier was about 80 kcal/mol,[24,25] which was too high compared to the free energy of the hydrolysis of MPD in solution (about 47 kcal/mol[7]).

Obviously, solvation effects contribute greatly to the hydrolysis reaction and should be taken into account. Recently, ab initio quantum mechanical (QM) calculations at various levels of theory combined with Langevin dipoles (LD) or Poisson−Boltzmann and/or polarized continuum (PCM) solvation models were used to consider the effects from solution.[4,9,10,13−15] Fundamental work done in Warshel's group concluded that the free energy of TSs for an associative pathway was comparable to the free energy of those for a dissociative pathway,[4,12] although an associative pathway with much lower free energy than the dissociative one was also proposed.[13] For associative pathways, two transition states (one with R1 = 1.92 Å and R2 = 2.22 Å and the other with R1 = 2.43 Å and R2 = 1.77 Å) with almost the same activation energy had been identified for the hydrolysis of MPD,[4] while the later work from the same group supported a single transition state, first at R1 = 1.8 Å and R2 = 2.0 Å[13] and later at R1 = 2.15 Å and R2 = 1.90 Å.[12] Despite the discrepancies in the structure of TS, all of these studies supported a concerted mechanism with single transition states and no intermediates for both associative and dissociative pathways, if not considering the potential proton transfers.

Besides the debates about the two alternative pathways, the mechanism of proton transfer (it could be from nucleophilic water to MPD or from the phosphate group to the leaving group) was also investigated.[4,12,14,26] The proposed mechanisms could be a stepwise process with H_{PT} first transferring to O_P to form a hydroxide ion, which then attacked the resulting methyl phosphate monoanion,[4] or a concerted proton transferred from the attacking water to the phosphate oxygen atom, during which the bond formation of P−O_W was completed.[7,12] Other proton transfer processes with the assistance of a bridging water were highlighted as well.[26,14]

To reconsider these findings, here, we solvated the MPD in explicit water molecules, thereby taking the solvation effects fully into account within a quantum mechanical and molecular mechanical approach.[27] Resorting to the newly introduced method, the multidimensional potential of mean constraint force (MPMCF), a two-dimensional free energy landscape along R1 and R2 was constructed. It supported the previous conclusion concerning comparable energetics of TSs for both pathways[4,12] and indicated a relatively flat free energy surface of the TS region from the associative TS to the dissociative TS. A detailed investigation of a proposed associative pathway suggested that the reaction involved at least five important reaction coordinates. Besides the traditional coordinates that were related to the bond of P−O_W and P−O_M, there were proton transfers and proton rotation involved. Our study suggests MPMCF as a powerful method to use in investigating a complex process involving multiple important coordinates.

METHOD

Quantum Mechanical and Molecular Mechanical Simulations. MPD was solvated into explicit water by quantum mechanical and molecular mechanical simulations.[27] The structure of MPD was built using Gaussian View and optimized at the level of B3LYP (6-31G*) in Gaussian 03.[28] The optimized MPD was then solvated together with nucleophilic water into a box of TIP4P water. The MPD molecule and the water molecule were described by QM at the level of B3LYP (6-31G*), while the remainder including 2842 TIP4P water molecules and 12 salt ions (seven sodium ions and five chloride ions to neutralize the negative charges in MPD) at a physiological concentration were described by the OPLS-AA force field.[29] In total, there were 11 392 atoms. The simulations were performed using Gromacs-4.0.7[30] with an interface to Gaussian 03.[28] The system was simulated as an NpT ensemble with a temperature of 300 K and a pressure of 1.0 bar using a thermal coupling to the Nose−Hoover thermostat[31,32] and an isotropic pressure coupling to a Parrinello−Rahman barostat.[33,34] Lennard-Jones interactions were estimated within a cutoff of 12 Å. Electrostatic interactions within a distance of 12 Å were calculated explicitly, while long-range electrostatic interactions were evaluated by particle-mesh Ewald summation.[35] The integration time step was 1 fs, and LINCS[36] (if not noted otherwise) was applied to all bonds that contained a hydrogen atom. The total simulation time was more than 10 ns (about 4×10^5 central processing unit hours).

Multidimensional Potential of Mean Constraint Force (MPMCF). From a theoretical point of view, the comparison of the free energy of TSs for associative and dissociative pathways in the hydrolysis of MPD could reveal unambiguously which pathway is more favored. The choice of an appropriate method to calculate free energies has to consider the extent of computations, especially for QM/MM simulation at the level of density functional theory, which is normally 3 or 4 orders of magnitude slower than classical molecular simulation. As initially suggested by van Gunsteren, free energy changes can be computed from the work performed by constraint forces.[37] Following this approach, the potential of the mean constraint force (PMCF) method was developed,[38−40] and then a new, concise formulation for free energy calculations based on constraint simulations was proposed[41−43] (for a review, see ref 43). In contrast to constrained simulations like PMCF, the adaptive biasing force (ABF) method was proposed to obtain a free energy surface from unconstrained simulations[44−46] and then extended to construct multidimensional free energy landscapes.[47,48] Instead, ABF applies an adaptive biasing force along the chosen order parameter and thus leads to a barrierless sampling. Umbrella sampling[49] and metadynamics[50] adapt a biased potential to enhance sampling and then derive free energy from the density of configurations. Recently, paradynamics used an empirical valence bond reference potential to accelerate the convergence to the actual free energy,[51] thus providing an efficient alternative for free energy estimation. Free energy perturbation (FEP) is another major way to compute free energy;[52] its recent improvement, free energy perturbation/umbrella sampling (FEP/US), specifically for QM/MM models was reviewed in ref 53. Here we have extended PMCF for the evaluation of multidimensional free energy surfaces.

The method constrains the system at certain points along a carefully chosen reaction coordinate (RC) r. The constraint force f_r^c is calculated, and the free energy along r is obtained via the formula

$$A(r) = \int \langle f_r^c \rangle_c \, d\mathbf{r} - k_B T \ln\langle z(r)^{-1/2} \rangle_c \quad (1)$$

Here, r is the variable along the path, A is the free energy, $\langle f_r^c \rangle_c$ is the mean constraint force along the RC that is computed as the corresponding Lagrange parameter $\langle \lambda_r \rangle_c$, and $z(r)$ is the Fixman determinant of the coordinate transformation used.[54] For details, please refer to refs 38 and 41.

Later, eq 1 was extended to eq 2 for the free energy along a one-dimensional reaction coordinate r_1 with multiple constraints imposed to further coordinates r_2, ..., r_n.[42] Here, $\mathbf{z}$ is the Fixman matrix of the coordinate transformation leading to the constrained system.[54] It depends on all constrained variables in which $\mathbf{r} = (r_1, r_2, ..., r_n)$. Free energy then depends on the RC as

$$A(r_1) = \int \langle f_1^c \rangle_c \, \mathrm{d}\mathbf{r} - k_B T \ln\langle (\det(\mathbf{z})^{-1/2}) \rangle_c \tag{2}$$

where the force now bears the index number of the RC.

Accordingly, free energy in the subspace of all n selected coordinates takes the form

$$A_n(r_1, ..., r_n) = \sum_{\alpha=1}^{n} \int \langle f_\alpha^c \rangle_c \, \mathrm{d}\mathbf{r}_\alpha - k_B T \ln\langle (\det(\mathbf{z})^{-1/2}) \rangle_c \tag{3}$$

which is a straightforward generalization of the previous expressions. It represents the free energy landscape in the subspace and is connected to the joint probability $P_n(r_1,...,r_n)$ by $P_n \propto \exp(-A_n/k_B T)$. In condensed form, it contains relevant statistical information about a high-dimensional system, which may not be available when considering only one particular, preselected RC that sometimes fails to describe a reaction. In practice, there are always several order parameters (formerly, we said reaction coordinates) that are important for chemical reactions and should be considered to understand the mechanism. Now, with eq 3, one can estimate the free energy difference between any two points in the free energy landscape. Reaction pathways can be detected without bias in the two- or three-dimensional subspace. In the application to MPD, the constraints are applied to internal coordinates such as interatomic distances, while the solute moves freely in the solvent. Thus, nonequilibrium solution effects are unlikely.[55] Application of eq 3 will be denoted as the multidimensional potential of mean constraint force (MPMCF) method. For computational details, see also the Supporting Information.

The evaluation of free energies using MPMCF can be divided easily into many independent and relatively short simulations. It is thus computationally feasible even for QM/MM simulations at a high level of theory. In addition, the choice of good order parameters can largely improve the efficiency of sampling, and the use of order parameters like the effective valence bond (EVB) energy gap, which has been shown to be a good reaction coordinate in FEP/US studies,[56,57] is of great interest for future MPMCF studies.

RESULTS AND DISCUSSION

Free Energy Surfaces Obtained from Different Metastable States. To construct the free energy surface (FES) for the hydrolysis of MPD in water, we started from different metastable states and evolved the system along different paths (for details, see Supporting Information). Figure 2 shows the obtained two-dimensional FESs. If R1 and R2 were the only two important coordinates for the hydrolysis, we could expect that the FESs obtained would be independent of the initial structures and the paths, along which the system was constrained. However, we found that the FESs obtained were quite different, and only part of FESs overlapped with each other. Thus, there must be other reaction coordinates that are fundamental to the hydrolysis that were ignored. In case of a significant difference between two FESs, there was at least another coordinate essential to the hydrolysis that was missing. By comparing the differences of the structures at those points between the two FESs, one could easily identify the missing coordinate that should be taken into account.

The initial structures of FESs shown in Figure 2A and B were both within the region of the reactant state with R1 = 1.80 Å and R2 = 3.60 Å. However, we found that there were obvious differences in the top-left region where R2 was less than 2.16 Å due to the different paths along which the mean constraint forces (MCF) were evaluated. For example, structures a and b are representative structures at R1 = 1.88 Å and R2 = 2.16 Å along the associative pathway for the two cases. The major difference between them is the position of H_{PT}, depending on whether or not the proton is transferred. Hence, the coordinates for the proton transfer from O_W to O_P should be taken into account to improve the FES. Similarly, the difference between FESs shown in Figure 2E and F, the initial structures of which were from the product region with R1 = 3.30 Å and R2 = 1.80 Å, are found in the top-left region with R1 $\leq$ 2.10 Å. Comparing the typical structures at R1 = 2.00 Å and R2 = 1.84 Å, structure e and f, revealed that the difference between the two was the position of H_{PT} and that the missing coordinate was the proton transfer from O_P to O_M. Also, FESs shown in Figure 2C and D (their initial structures were those with R1 = 1.80 Å, R2 = 1.64 Å and R1 = 1.64 Å, R2 = 1.80 Å, respectively) show a large difference in the top-left region. Structures c and d are representative structures taken at R1 = 1.84 Å and R2 = 1.84 Å. The difference between the two structures was more subtle, just lying in the orientation of the bond between O_P and H_{PT}. In structure c, the O_P–H_{PT} bond was orientated toward O_W, while in structure d, it was orientated toward O_M. Here, we proposed a rotation of the O_P–H_{PT} bond from one side of the phosphate plane to the other without any bond formation or bond cleavage, nevertheless involving a large free energy contribution.

The Fixman determinant in eq 3 was taken into account everywhere when calculating the free energy surfaces. The correction generally yielded a small, but not negligible, contribution to free energy. For instance, in the first example shown in Figure 2, the maximum is found at point R1 = 3.70 Å, R2 = 3.60 Å and the minimum at R1 = 1.64 Å, R2 = 1.64 Å, the difference being about 1 kcal/mol, which is small when compared to the total free energy difference. The calculated values are shown in Table S5.

Coordinates of Proton Transfer. As revealed by the above analysis, the proton transfer from either O_W to O_P or from O_P to O_M was important for the hydrolysis of MPD. The corresponding distances, $X1$ and $X2$, were defined in Figure 2. What we considered next was where the proton transfer took place and how the free energy landscape along the coordinate of proton transfer looked. In the case of the proton transfer from O_W to O_P, we constructed the free energy landscape along X by maintaining the R1 and R2 coordinates constant and varying the coordinate of proton transfer $X = X2^2 - X1^2$ (method details are given in the Supporting Information). To determine where the proton transfer occurred, we checked the free energy landscape of four paths between two fixed points (R1 = 1.80 Å, R2 = 2.20 Å and R1 = 1.80 Å, R2 = 2.12 Å. Their representative structures are structure b and d in Figure 3, respectively).

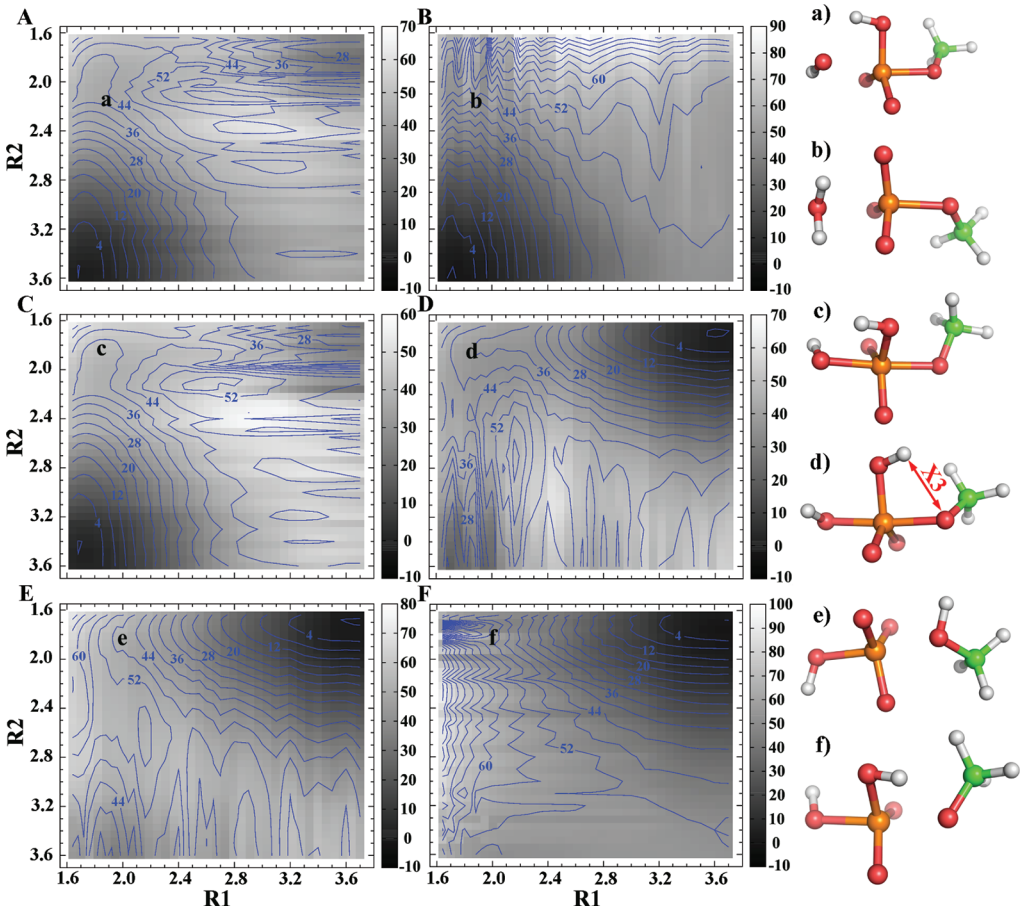

Figure 2. Two-dimensional free energy surfaces along R1 and R2. Left: A, B, C, D, E, and F are the free energy surfaces evaluated by MPMCF starting from different initial structures and/or along different integral paths. For example, A/B differ from C/D and E/F in the initial structures used, while A/C/E differ from B/D/F in the defined integral paths. The initial structures and the defined integral paths are listed in Table S3, and the steps to construct the FESs are explained in the Supporting Information. Right: Structures a and b are the representative structures at R1 = 1.88 Å and R2 = 2.16 Å in A and B, respectively. Structures c and d are the representative structures at R1 = 1.84 Å and R2 = 1.84 Å in C and D, respectively. Structures e and f are the representative structures at R1 = 2.00 Å and R2 = 1.84 Å in E and F, respectively. The locations of all of the structures are highlighted correspondingly in FESs of the left side. An important reaction coordinate X3, the distance between H_{PT} and O_M, is highlighted in structure d.

The four paths concerned the proton transfer from four different points (with R1 = 1.80 Å and R2 = 2.12 Å, 2.14 Å, 2.16 Å, and 2.20 Å, respectively). The free energy landscapes are shown in inset II of Figure 3. Since the free energy difference between two points in the FES is independent of the integral paths, the free energy difference between the two fixed points that were obtained along the four paths should be the same. As shown in inset II of Figure 3, the free energy differences between the two fixed points obtained along the four different paths were quite close (within the standard deviation of 0.84 kcal/mol). This demonstrated the accuracy of MPMCF. The barrier appeared at some point in the middle of the proton transfer. For example, the energy barrier in the case of R2 = 2.16 Å was at $X = 0.11$ Å^2, and a representative structure is shown in Figure 3 (structure c). However, the energy barrier became lower as R1 increased (see Figure S7A). We propose that, as R1 increases, there should be a point at which the barrier was lower than the energy at the end point (R1 = 1.80 Å, R2 = 2.12 Å) and that the proton transfer occurred by simply climbing the free energy barrier. It was the saddle point in the FES concerning the coordinate of proton transfer at which the proton transferred from the attacking water directly to MPD during the nucleophilic attack.

To confirm the exact point where the proton transfers, we performed transition path sampling[58] (for method details, see the Supporting Information). A direct proton transfer from O_W to O_P was observed, and the O_W−P bond formed almost at the same time (see Figure S4). The concerted proton transfer was in good agreement with the results obtained from the study that combined FEP calculation and EVB potential approximation.[12] The inverse dependence of the hydrolysis rate on the concentration of hydroxide that was observed experimentally also supported the existence of a monoanion and, thereby, the contribution of the proton transfer to the hydrolysis.[7] The proton transfer took place in a broad range of R2 from 2.25 Å to 2.95 Å (see Figure S5). The proton was transferred at an average point of R1 = 1.71 ± 0.05 Å, R2 = 2.54 ± 0.12 Å. The result confirmed the above-mentioned prediction from Figure S7A that proton transfer should occur at some point with R1 > 2.2 Å.

In the case of proton transfer from O_P to O_M, the reaction coordinate of the proton transfer was taken as $Y = X3^2 - X1^2$, with X3 being the distance between H_{PT} and O_M (see Figure 2). Similarly, the free energy difference between two points (R1 = 2.18 Å, R2 = 1.80 Å and R1 = 2.25 Å, R2 = 1.80 Å and their representative structures were structures h and j in Figure 3,

dx.doi.org/10.1021/ct300022m | J. Chem. Theory Comput. 2012, 8, 3596−3604

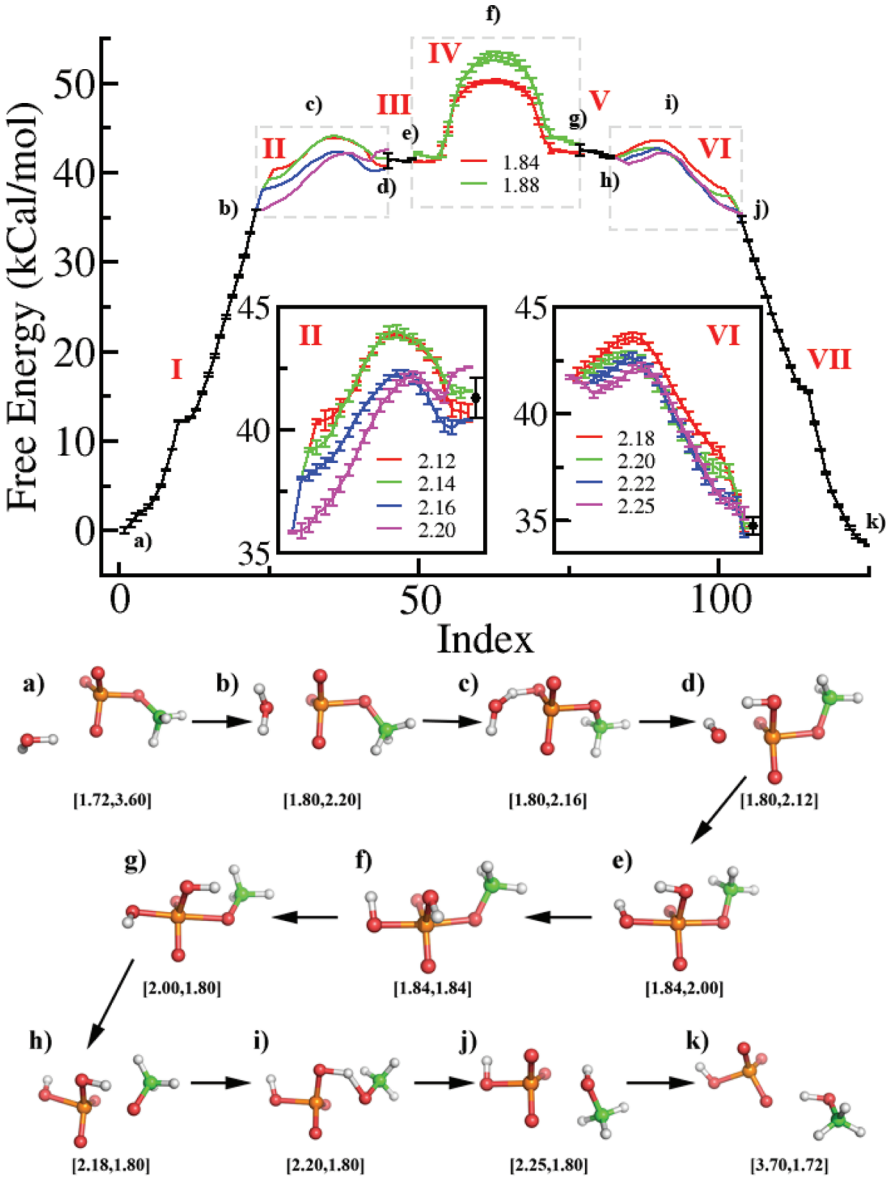

Figure 3. Free energy landscape along a representative associative pathway. The associative pathway is represented by a sequence of states. The *X* axis is the index in the sequence of states, and the *Y* axis is the corresponding free energy (see Table S1). The pathway consists of seven steps from I to VII. The insets II and VI show the respective free energies along four paths as enlarged drawings. Their average over the end states is highlighted as a black dot. The numbers shown in the legend of the inset II (VI) correspond to the values of R2 (R1). In step IV, the free energies along two paths are evaluated. Structures a, b, d, e, g, h, j, and k are the representative structures in the beginning and ending of each step, structures c, f, and i are three representative structures in the middle of steps II, IV, and VI, respectively. Their positions in the free energy landscape are also shown. The numbers below each structure are [R1, R2]. Error bars give the standard deviation.

respectively) was evaluated along four different paths, in which the points for proton transfer were at R2 = 1.80 Å and R1 = 2.18 Å, 2.20 Å, 2.22 Å, and 2.25 Å, respectively. The resulting free energy landscape is shown in inset IV of Figure 3. The free energy differences calculated along the four paths were consistent within the standard deviation of 0.38 kcal/mol. As observed above, an energy barrier appeared during the proton transfer, and it became lower as the methyl group moved farther away (see Figure S7B). Structure i in Figure 3 is a representative structure that was lying in the energy barrier with $Y = 0.55$ Å^2 in the case of R1 = 2.20 Å. As in the previous case, there should be a point where the proton transfer is simply a process of sliding down the free energy landscape as the methyl group moves further apart.

Rotation of the O_P–H_{PT} Bond. From structure c to structure d in Figure 2 (the two structures with opposite orientation of the O_P–H_{PT} bond), a possible mechanism could be the transfer of H_{PT} to the bulk water, followed by the uptake of a proton from the bulk water on the other side. However, the cleavage and formation of an O–H bond usually involves a very high energy barrier and appears unlikely. Here, we instead propose a rotation of the O_P–H_{PT} bond. The rotation of an O–H bond was reported in studies of related systems such as the hydrolysis of phosphodiesters by several nucleophiles,[5] the neutral cyclic oxyphosphorane,[59] and the attack of methanol on ethylene phosphate.[60] We defined $Z = X2^2 - X3^2$ as an approximation of the rotation coordinate (X2 was defined in Figure 1, X3 in Figure 2). As in the case of proton transfer, the free energy along the rotation coordinate was estimated by

dx.doi.org/10.1021/ct300022m | J. Chem. Theory Comput. 2012, 8, 3596–3604

keeping R1 and R2 invariant and varying Z. The free energy landscapes between two points (R1 = 1.84 Å, R2 = 2.00 Å and R1 = 2.00 Å, R2 = 1.80 Å and their representative structures are structures e and g in Figure 3, respectively) were estimated along two rotation paths. One initiated from R1 = 1.84 Å, R2 = 1.84 Å (the red curve in Figure 3 phase IV) and the other from R1 = 1.88 Å, R2 = 1.88 Å (the green curve in Figure 3 phase IV). Although the free energies of the end point in phase IV (R1 = 2.00 Å, R2 = 1.80 Å) are integrated along two paths, they are expected to be the same. Here, we find that they are very close, with a small difference of 1.2 kcal/mol (see Table S2 step IV). This again demonstrates the accuracy of our method. As shown in Figure 3, phase IV (see also Table S2 step IV), the energy barrier of rotation initiated from R1 = 1.84 Å, R2 = 1.84 Å is 50.2 kcal/mol, which is 2.8 kcal/mol smaller than the one initiated from R1 = 1.88 Å, R2 = 1.88 Å (53.0 kcal/mol). We note that we did not systematically evaluate the free energy barrier for the rotation of the OH bond. Thus, we cannot exclude a point at which the rotation took place with an energy barrier lower than the one at R1 = 1.84 Å, R2 = 1.84 Å (50.2 kcal/mol), which therefore can be only considered as an upper bound of the energy barrier.

Other mechanisms to reorient the proton toward the leaving group may involve a pseudorotation.[5,59,60] This pathway cannot be ruled out here and is of high interest for future investigations.

A Complete Associative Pathway. Realizing the discontinuity of the 2-D free energy landscape along R1 and R2, we propose a detailed associative pathway, which involves seven steps, including two proton transfers and a rotation of the O−H bond. We chose many states to represent the path, which was expressed as an ordered sequence of states, $P(N) \equiv \{X_1, X_2, ..., X_N\}$ (see Table S1). To ensure the reversibility of the path, we checked the reversibility of every single step, say between X_i and X_{i+1}, by comparing the constraint mean forces (CMF) and the structures from X_i to X_{i+1} (forward) and those from X_{i+1} to X_i (backward). We found that CMF and the structures of both forward and backward simulations were consistent. So, the associative path that we evaluated here was reversible, and all important reaction coordinates were taken into account. Thus, the free energy that we obtained here is reliable.

The free energy results are shown in Figure 3. The seven steps are labeled from I to VII, and the computational details for each step are shown in the Supporting Information. (I) First, starting from the reactant state (Figure 3, structure a), the water attacks the phosphate group as R2 decreases and ends with structure b in Figure 3. (II) Then, H_{PT} transfers to O_P to reach structure d in Figure 3, and (III) the bond between O_W and P forms to end with a pentacoordinated structure (Figure 3, structure e). (IV) The $H_{PT}-O_P$ bond needs to rotate from one side of the phosphate plane to the other side to form another pentacoordinated structure (Figure 3, structure g) by (V) passing the overall transition state TS (Figure 3, structure f). (VI) The $P-O_M$ bond is then cleaved (Figure 3, structure h). Now, H_{PT} can transfer from the phosphate group to the methanol group (Figure 3, structure j), after which (VII) the methanol group moves farther away with R1 increasing from 2.25 Å to 3.70 Å, and the product state (PS) is formed (Figure 3, structure k). For proton transfer and the rotation of the O−H bond, the free energy was evaluated along different paths, and the free energy of the end point was taken as the average of them. As discussed above, the actual points where the proton was transferred were different from the ones in these proposed paths. However, the relative free energy for step III (step V) should be independent of the proton transfer paths in step II (step VI), along which the free energy is estimated. Surprisingly, the transition state of the hydrolysis along an associative pathway was the one during the rotation of the O−H bond and was estimated to be at most 50.2 kcal/mol (the energy barrier estimated from point R1 = 1.84 Å and R2 = 1.84 Å). This is consistent with the experimental results (47 kcal/mol).[7] Therefore, the suggested point for the rotation of the O−H bond should be quite close to the actual point if not exactly there. Most of the overall barrier is, however, due to the formation of a planar PO_3 moiety on the way to the penta-coordinated intermediate. In previous theoretical results, the transition state that was identified might not be the overall transition state, due to ignoring the rotation of the O−H bond. If one does not consider the rotation coordinate, the transition state for the associative state was at R1 = 2.00 Å and R2 = 1.80 Å (see Figure S2) with a relative free energy of 42.5 kcal/mol. This is quite close to the transition structure proposed for the associative pathway in ref 12 with R1 = 2.15 Å and R2 = 1.90 Å and a relative free energy of 41.1 kcal/mol.

Estimation of the 2-D Free Energy Surface. As mentioned before, only part of the FESs shown in Figure 2 are close to the actual FES due to having ignored the other important coordinates. For example, the lower-left triangular part of the FESs in Figure 2A and B and the upper-right triangular part of the FESs in Figure 2E and F are resolved faithfully. The idea is to piece together these faithful parts to gain a more accurate picture of the FES. Taking the free energy landscape in Figure 3 as a reference, we combined the FESs in Figure 2A, B, E, and F into a two-dimensional FES (see Figure 4)

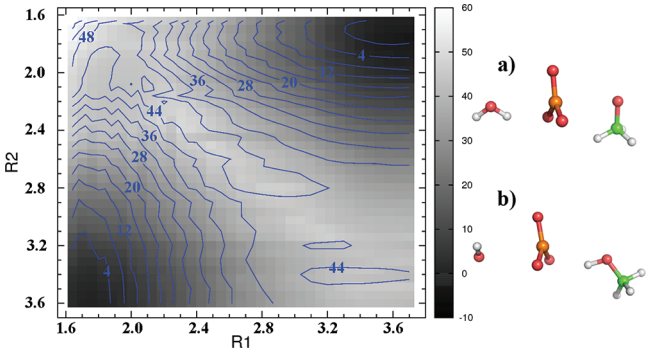

Figure 4. The free energy surface along R1 and R2 by integrating four free energy surfaces shown in Figure 2. Structures a and b are the representative structures at R1 = 3.50 Å and R2 = 3.50 Å in Figure 2B and F, respectively.

along R1 and R2 by taking the lowest free energy among them. (Why these four FESs can be combined given that they are constructed from different initial structures and how they were combined are explained in the Supporting Information).

As one would expect, the lower-left triangular part of this FES was taken mainly from the lower-left triangular part of Figure 2A and B, while the upper-right triangular part was taken from the corresponding part of Figure 2E and F. These two parts met in the diagonal part of the FES. In this FES, the point at which the proton transfer takes place is not the actual point, but around R1 $\leq$ 2.12 Å. The proton transfer was found to take place within 1 ps at that point, and its barrier could be very small. For example, the energy barrier for proton transfer at point R1 = 1.80 Å and R2 = 2.12 Å is about 3 kcal/mol; more

dx.doi.org/10.1021/ct300022m | J. Chem. Theory Comput. 2012, 8, 3596−3604

importantly, the free energies for the states before proton transfer and after proton transfer are almost the same (see Figure 3). Thus, the free energy estimated is still quite reliable without exploring the proton transfer coordinate, given that the free energy difference between two points is independent to the integral path. In the upper-right triangular part, the rotation of the O−H bond would be the main coordinate that is missing. The lower-right part of the FES should involve a complex process from structure a to structure b in Figure 4, which could be the proton transfer via water bridges to methanol. Structure a was a representative structure at R1 = 3.50 Å, R2 = 3.50 Å in Figure 2B, and structure b was the one at the same point as in Figure 2F, both of which correspond to a dissociative pathway. Assuming that the free energy barriers for the missing coordinates are the same, the FES in Figure 4 should reflect the overall shape of the real FES in the diagonal part. Thus, consistent with the previous results,[4,12] Figure 4 shows that the associative mechanism was indistinguishable from the dissociative one, with comparable free energy barriers. Although the common view is that the dissociative and associative pathways are separated by a high energy barrier,[12] we here suggest another possibility, namely, that the hydrolysis of the MPD could occur not only through typical associative, dissociativ,e and concerted pathways but also through intermediate pathways between them. The validation requires a free energy surface resolved along the coordinate of proton transfer and other important coordinates.

Lateral Attacking S_N2 Pathway. Another possible mechanism of the hydrolysis of MPD is the nucleophilic attack of MPD by water from the same side as the leaving group. In this case, the proton of the water would transfer directly to the methyl group. We proposed a three-step S_N2 path, along which the free energy landscape was then estimated (see Figure 5 and Supporting Information). First, (1) the attacking water climbs up along the free energy barrier to approach the phosphate group (from structures a to b in Figure 5). Then, (2) H_{PT} transfers from O_W to O_M (from structures b to d in Figure 5 and possibly via a transition state analogue to structure c in Figure 5). Finally, the O_W−P bond forms, but meanwhile the O_M−P bond breaks. Then, the methyl group moves far away (from structure d to structure e in Figure 5). Here, the coordinate for proton transfer was chosen as $Y = X3^2 - X2^2$. The free energy landscape between point R1 = 2.30 Å, R2 = 2.30 Å and R1 = 2.30 Å, R2 = 2.20 Å was evaluated via proton transfer at four different points (with R1 and R2 are [2.30 Å, 2.30 Å], [2.20 Å, 2.30 Å], [2.20 Å, 2.20 Å], and [2.30 Å, 2.20 Å], respectively). The estimated free energy differences between these two points were consistent with a deviation of 0.9 kcal/mol (see the inset II in Figure 5). By comparing the free energy barrier between proton transfers at different points, it is difficult to determine where the proton transfers. However, the overall free energy barrier was around 60−62 kcal/mol, which is about 10 kcal/mol higher than the free energy barrier along the associative paths proposed above. So, this lateral attacking pathway can be excluded on the basis of our calculations.

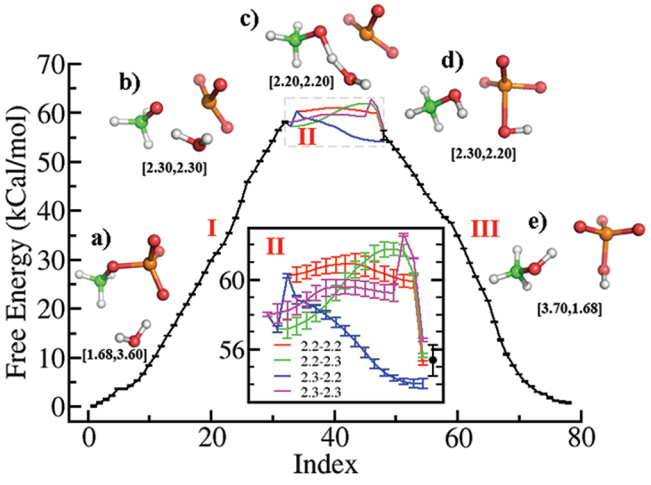

Figure 5. The free energy landscape along a lateral attacking pathway. The *X* and *Y* axes are the same as in Figure 3 (see Table S2 for the details). The pathway consists of three steps, which are labeled from I to III. The inset II is the magnification of step II. In step II, the free energies along four paths are evaluated; their average over the last point is finally taken and highlighted as black dots shown in inset II. The numbers shown in the legend of inset II correspond to the values of R1 and R2 with the form of [R1−R2]. Structures a, b, d, and e are the representative structures in the beginning and at the end of each step, whereas structure c is a representative structure near the energy barrier during the rotation of the O−H bond at R1 = 2.20 Å and R2 = 2.20 Å in step II. The pair of numbers below each structure are its values of R1 and R2 with the form of [R1, R2]. The error bar is the standard deviation.

CONCLUSION

The mechanism of the hydrolysis of MPD was investigated by QM/MM simulation. The reactants were described by the DFT method at the level of B3LYP (6-31G*), and explicit water was used to take the solvation effect into account, unlike the adaptation of implicit water in previous theoretical studies.[4,9,10,13−15] A newly developed method, MPMCF, was used to construct the FES along two traditionally important coordinates—R1 and R2. Using this method, accurate free energy landscapes were estimated along three-dimensional paths as well. On the basis of these, a clearer picture of the mechanism was gained. (1) By combining four different FESs with different initial structures and integral paths, a 2-D FES was constructed along R1 and R2 and shown to feature a flat TS region. Consistent with previous theoretical results,[4,12] this supports the view that associative and dissociative pathways are indistinguishable and similarly visited. In addition, we suggest that the pathways lying between the associative and dissociative pathways are equally favored. In biological systems, a hydrolytic enzyme might adapt to one specific structure of those transition states to selectively catalyze the hydrolysis reaction. (2) In combination with transition path sampling, a detailed investigation of proton transfer revealed the exact moments when the proton transfers occur. We suggest a direct proton transfer from the water to the phosphate group or from the phosphate group to methyl, combined with the formation of the O_W−P bond or the cleavage of the O_M−P bond, respectively. The formerly proposed two-step attacking mechanism (water is first deprotonated to the OH^-, which then attacks the phosphate group) was ruled out. (3) A new coordinate, the rotation of the O_P−H_{PT} bond, was identified as being important along the associative pathway. Finally, the TS for the whole associative pathway was located during the rotation of the O_P−H_{PT} bond. The free energy of the identified TS was 50.2 kcal/mol and therefore consistent with experimental data.[7] (4) MPMCF is a novel method to construct the multidimensional free energy landscape of a system, which is feasible even for QM/MM simulation with DFT methods. By scanning along a specific coordinate, the MPMCF was similar to a relax scan in quantum mechanical calculation. A method that is similar to the intrinsic

reaction coordinate method[61] might be adapted to MPMCF. It would facilitate the identification of transition states in molecular simulations. Furthermore, MPMCF can estimate the free energy difference of two points in multidimensional (here three-dimensional) FES at moderate computational costs and thus provides a powerful method to decipher the mechanism of complex processes that involve many important coordinates.

■ ASSOCIATED CONTENT

Supporting Information

Other details of the MPMCF and TPS methods and important results including figures and tables are given. This material is avilable free of charge via the Internet at http://pubs.acs.org/.

■ AUTHOR INFORMATION

Corresponding Author

*E-mail: frauke.graeter@h-its.org; juergen.schlitter@rub.de.

Notes

The authors declare no competing financial interest.

■ ACKNOWLEDGMENTS

The authors thank the Department of Theoretical and Computational Biophysics of the Max-Plank-Institute for Biophysical Chemistry for providing the computational power to complete most of the free energy calculations. We are thankful for the financial support by the Klaus Tschira Foundation and the Sino-German Junior Research Group program. In addition, W.L. is grateful for an MPG-CAS Ph.D. scholarship.

■ REFERENCES

(1) Cleland, W.; Hengge, A. *Chem. Rev.* **2006**, *106*, 3252−3278.
(2) Vetter, I.; Wittinghofer, A. *Q. Rev. Biophys.* **1999**, *32*, 1−56.
(3) Westheimer, F. *Chem. Rev.* **1981**, *81*, 313−326.
(4) Florián, J.; Warshel, A. *J. Phys. Chem. B* **1998**, *102*, 719−734.
(5) Lopez, X.; Dejaegere, A.; Leclerc, F.; Darrin, M.; Karplus, M. *J. Phys. Chem. B* **2006**, *110*, 11525−11539.
(6) Klähn, M.; Mathias, G.; Kötting, C.; Nonella, M.; Schlitter, J.; Gerwert, K.; Tavan, P. *J. Phys. Chem. A* **2004**, *108*, 6186−6194.
(7) Lad, C.; Williams, N.; Wolfenden, R. *Proc. Natl. Acad. Sci. U.S.A.* **2003**, *100*, 5607−5610.
(8) Friedman, J.; Freeman, S.; Knowles, J. *J. Am. Chem. Soc.* **1988**, *110*, 1268−1275.
(9) Florián, J.; Warshel, A. *J. Am. Chem. Soc.* **1997**, *119*, 5473−5474.
(10) Florián, J.; Åqvist, J.; Warshel, A. *J. Am. Chem. Soc.* **1998**, *120*, 11524−11525.
(11) Wolfenden, R.; Ridgway, C.; Young, G. *J. Am. Chem. Soc.* **1998**, *120*, 833−834.
(12) Kamerlin, S.; Florián, J.; Warshel, A. *ChemPhysChem* **2008**, *9*, 1767−1773.
(13) Klähn, M.; Rosta, E.; Warshel, A. *J. Am. Chem. Soc.* **2006**, *128*, 15310−15323.
(14) Bianciotto, M.; Barthelat, J.; Vigroux, A. *J. Am. Chem. Soc.* **2002**, *124*, 7573−7587.
(15) Wang, Y.; Topol, I.; Collins, J.; Burt, S. *J. Am. Chem. Soc.* **2003**, *125*, 13265−13273.
(16) Jencks, W. *Chem. Rev.* **1985**, *85*, 511−527.
(17) ÓFerrall, R. *J. Chem. Soc. B* **1970**, 274−277.
(18) Williams, A. *Adv. Phys. Org. Chem.* **1992**, *27*, 1−55.
(19) Jencks, W. P. *Catalysis in Chemistry and Enzymology*; McGraw-Hill, New York, 1969.
(20) Kirby, A.; Jencks, W. *J. Am. Chem. Soc.* **1965**, *87*, 3209−3216.
(21) Kirby, A.; Varvoglis, A. *J. Am. Chem. Soc.* **1967**, *89*, 415−423.
(22) Hoff, R.; Hengge, A. *J. Org. Chem.* **1998**, *63*, 6680−6688.
(23) Åqvist, J.; Kolmodin, K.; Florián, J.; Warshel, A. *Chem. Biol.* **1999**, *6*, R71−R80.
(24) Zhou, D.; Taira, K. *Chem. Rev.* **1998**, *98*, 991−1026.
(25) Dejaegere, A.; Liang, X.; Karplus, M. *J. Chem. Soc., Faraday Trans.* **1994**, *90*, 1763−1770.
(26) Hu, C.; Brinck, T. *J. Phys. Chem. A* **1999**, *103*, 5379−5386.
(27) Groenhof, G.; Bouxin-Cademartory, M.; Hess, B.; De Visser, S. P.; Berendsen, H. J.; Olivucci, M.; Mark, A. E.; Robb, M. A. *J. Am. Chem. Soc.* **2004**, *126*, 4228−4233.
(28) Frisch, M. J.; Trucks, G. W.; Schlegel, H. B.; Scuseria, G. E.; Robb, M. A.; Cheeseman, J. R.; Montgomery, J. A. Jr.; Vreven, T.; Kudin, K. N.; Burant, J. C.; Millam, J. M.; Iyengar, S. S.; Tomasi, J.; Barone, V.; Mennucci, B.; Cossi, M.; Scalmani, G.; Rega, N.; Petersson, G. A.; Nakatsuji, H.; Hada, M.; Ehara, M.; Toyota, K.; Fukuda, R.; Hasegawa, J.; Ishida, M.; Nakajima, T.; Honda, Y.; Kitao, O.; Nakai, H.; Klene, M.; Li, X.; Knox, J. E.; Hratchian, H. P.; Cross, J. B.; Bakken, V.; Adamo, C.; Jaramillo, J.; Gomperts, R.; Stratmann, R. E.; Yazyev, O.; Austin, A. J.; Cammi, R.; Pomelli, C.; Ochterski, J. W.; Ayala, P. Y.; Morokuma, K.; Voth, G. A.; Salvador, P.; Dannenberg, J. J.; Zakrzewski, V. G.; Dapprich, S.; Daniels, A. D.; Strain, M. C.; Farkas, O.; Malick, D. K.; Rabuck, A. D.; Raghavachari, K.; Foresman, J. B.; Ortiz, J. V.; Cui, Q.; Baboul, A. G.; Clifford, S.; Cioslowski, J.; Stefanov, B. B.; Liu, G.; Liashenko, A.; Piskorz, P.; Komaromi, I.; Martin, R. L.; Fox, D. J.; Keith, T.; Al-Laham, M. A.; Peng, C. Y.; Nanayakkara, A.; Challacombe, M.; Gill, P. M. W.; Johnson, B.; Chen, W.; Wong, M. W.; Gonzalez, C.; Pople, J. A. *Gaussian 03*, revision C.02; Gaussian, Inc.: Wallingford, CT, 2004.
(29) Jorgensen, W. L.; Maxwell, D. S.; Tirado-Rives, J. *J. Am. Chem. Soc.* **1996**, *118*, 11225−11236.
(30) Hess, B.; Kutzner, C.; van der Spoel, D.; Lindahl, E. *J. Chem. Theory Comput.* **2008**, *4*, 435−447.
(31) Nose, S. *Mol. Phys.* **1984**, *52*, 255−268.
(32) Hoover, W. G. *Phys. Rev. A* **1985**, *31*, 1695−1697.
(33) Parrinello, M.; Rahman, A. *J. Appl. Phys.* **1981**, *52*, 7182−7190.
(34) Nose, S.; Klein, M. L. *Mol. Phys.* **1983**, *50*, 1055−1076.
(35) Darden, T.; York, D.; Pedersen, L. *J. Chem. Phys.* **1993**, *98*, 10089−10092.
(36) Hess, B.; Bekker, H.; Berendsen, H. J. C.; Fraaije, J. G. E. M. *J. Comput. Chem.* **1997**, *18*, 1463−1472.
(37) van Gunsteren, W. F.; Beutler, T. C.; Fraternali, F.; King, P. M.; Mark, A. E.; Smith, P. E. In *Computer Simulation of Biomolecular Systems: Theoretical and Experimental Applications*; van Gunsteren, W. F., Weiner, P. K., Wilkinson, A. J., Eds.; Escom Science Publisher: Leiden, The Netherlands, 1993; Vol. 2, Chapter: Computation of Free Energy in Practice: Choice of Approximations and Accuracy Limiting Factors, pp 315−348.
(38) Mülders, T.; Krüger, P.; Swegat, W.; Schlitter, J. *J. Chem. Phys.* **1996**, *104*, 4869−4870.
(39) Den Otter, W.; Briels, W. *J. Chem. Phys.* **1998**, *109*, 4139−4146.
(40) Sprik, M.; Ciccotti, G. *J. Chem. Phys.* **1998**, *109*, 7737−7744.
(41) Schlitter, J.; Klähn, M. *J. Chem. Phys.* **2003**, *118*, 2057.
(42) Schlitter, J.; Klähn, M. *Mol. Phys.* **2003**, *101*, 3439−3443.
(43) Schlitter, J. *Eur. Phys. J. Special Topics* **2011**, *200*, 91−105.
(44) Darve, E.; Pohorille, A. *J. Chem. Phys.* **2001**, *115*, 9169−9183.
(45) Darve, E.; Wilson, M.; Pohorille, A. *Mol. Simulat.* **2002**, *28*, 113−144.
(46) Darve, E.; Rodrguez-Gómez, D.; Pohorille, A. *J. Chem. Phys.* **2008**, *128*, 144120−144132.
(47) Hènin, J.; Fiorin, G.; Chipot, C.; Klein, M. *J. Chem. Theory Comput.* **2009**, *6*, 35−47.
(48) Chipot, C.; Lelièvre, T. Arxiv preprint arXiv:1008.3457, 2010.
(49) Torrie, G.; Valleau, J. *J. Comput. Phys.* **1977**, *23*, 187−199.
(50) Laio, A.; Parrinello, M. *Proc. Natl. Acad. Sci. U.S.A.* **2002**, *99*, 12562.
(51) Plotnikov, N.; Kamerlin, S.; Warshel, A. *J. Phys. Chem. B* **2010**, *115*, 7950−7962.
(52) Zwanzig, R. *J. Chem. Phys.* **1954**, *22*, 1420−1426.
(53) Kamerlin, S.; Haranczyk, M.; Warshel, A. *J. Phys. Chem. B* **2008**, *113*, 1253−1272.

(54) Fixman, M. *Proc. Natl. Acad. Sci. U.S.A.* **1974**, *71*, 3050−3053.
(55) Štrajbl, M.; Florián, J.; Warshel, A. *J. Phys. Chem. B* **2001**, *105*, 4471−4484.
(56) Xiang, Y.; Warshel, A. *J. Phys. Chem. B* **2008**, *112*, 1007−1015.
(57) Mones, L.; Kulhánek, P.; Simon, I.; Laio, A.; Fuxreiter, M. *J. Phys. Chem. B* **2009**, *113*, 7867−7873.
(58) Bolhuis, P. G.; Chandler, D.; Dellago, C.; Geissler, P. L. *Annu. Rev. Phys. Chem.* **2002**, *53*, 291−318.
(59) Uchimaru, T.; Uebayasi, M.; Hirose, T.; Tsuzuki, S.; Yliniemelä, A.; Tanabe, K.; Taira, K. *J. Org. Chem.* **1996**, *61*, 1599−1608.
(60) Lim, C.; Tole, P. *J. Am. Chem. Soc.* **1992**, *114*, 7245−7252.
(61) Fukui, K. *Acc. Chem. Res.* **1981**, *14*, 363−368.